INSTITUTE OF PHYSICS PUBLISHING INVERSE PROBLEMS

Inverse Problems **21** (2005) S65–S79 doi:10.1088/0266-5611/21/6/S06

Retrieval of inhomogeneous targets from experimental frequency diversity data

A Dubois[1], **K Belkebir**[2] **and M Saillard**[3]

[1] Université Paul Cézanne, Aix-Marseille III, Institut Fresnel, UMR-CNRS 6133, Campus de Saint Jérôme, Case 162, 13397 Marseille Cedex 20, France
[2] Université de Provence, Aix-Marseille I, Institut Fresnel, UMR-CNRS 6133, Campus de Saint Jérôme, Case 162, 13397 Marseille Cedex 20, France
[3] LSEET, UMR-CNRS 6017, Université du Sud Toulon-Var, BP 132, 83957 La Garde Cedex, France

E-mail: kamal.belkebir@fresnel.fr

Received 15 April 2005, in final form 30 August 2005
Published 25 November 2005
Online at stacks.iop.org/IP/21/S65

Abstract

The present paper deals with the reconstruction of two-dimensional permittivity and conductivity distributions from experimental multiple-frequency data. Three new iterative inverse schemes are described and compared. A frequency-weighted cost functional is introduced and minimizing this cost function rather than a standard one lead to a robust and accurate inverse algorithm. In addition, none of the three schemes uses a regularization procedure.

(Some figures in this article are in colour only in the electronic version)

1. Introduction

In this paper, the inverse scattering problem is addressed with iterative approaches based on the minimization of a cost functional involving multiple-frequency data. Results are compared with a frequency-hopping approach [1, 2] which requires a single-frequency inversion at each hopping step and has been successfully applied to real data [3], as described in the special section [4].

2. Statement of the problem and notation

The geometry of the problem is depicted in figure 1. A two-dimensional target of arbitrary cross section is confined in a bounded domain $\Omega \in \mathbb{R}^2$. The electromagnetic constants of the embedding medium are ε_0 and μ_0 (ε_0 and μ_0 being the permittivity and permeability of vacuum, respectively). The scatterers are assumed to be inhomogeneous dielectric and/or conducting cylinders of relative permittivity $\varepsilon_r(\mathbf{r})$, of conductivity $\sigma(\mathbf{r})$ and non-magnetic ($\mu(\mathbf{r}) = \mu_0$). A right-handed Cartesian coordinate frame $(O, \boldsymbol{u}_x, \boldsymbol{u}_y, \boldsymbol{u}_z)$ is defined. The

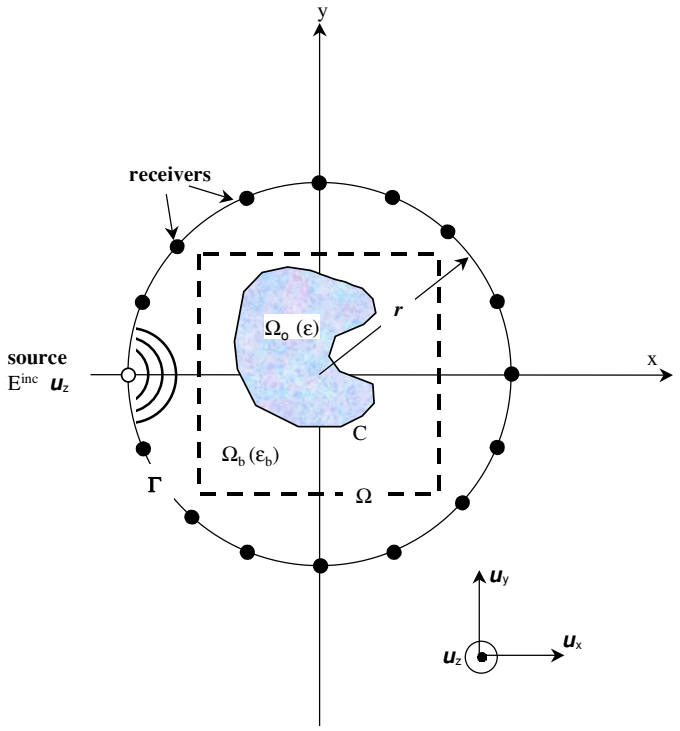

Figure 1. Geometry of the problem.

z-axis is parallel to the invariance axis of the cylinders. The position vector **OM** can then be written as

$$\mathbf{OM} = x\boldsymbol{u}_x + y\boldsymbol{u}_y + z\boldsymbol{u}_z = \mathbf{r} + z\boldsymbol{u}_z. \tag{1}$$

Targets under test are successively illuminated by $l = 1, \ldots, L$ electromagnetic sources generating successively a time harmonic field for $p = 1, \ldots, P$ operating frequencies. The sources are assumed to be infinite lines parallel to the z-axis and located at $(\mathbf{r}_l)_{1<l<L}$ all around the object. Taking into account a time dependence in $\exp(+\mathrm{i}\omega t)$, the TM-polarized incident field radiated by the lth source located at $\mathbf{r}_l$ for the pth frequency f_p is given by

$$\mathbf{E}^{\mathrm{inc}}_{l,p}(\mathbf{r}) = E^{\mathrm{inc}}_{l,p}(\mathbf{r})\mathbf{u}_z = A_p \frac{\omega_p \mu_0}{4} H_0^{(2)}(k_{0,p}|\mathbf{r} - \mathbf{r}_l|)\mathbf{u}_z, \tag{2}$$

where A_p is the strength of the current through the line source for the frequency f_p, ω_p is the angular frequency ($\omega_p = 2\pi f_p$), $H_0^{(2)}$ represents the Hankel function of zero order and of second kind and $k_{0,p}$ is the wave number in vacuum at the frequency f_p.

The scattered field is measured at M receivers located around the cylinders on a line Γ. At the frequency f_p and for the source l, the direct problem can be formulated as two coupled integral equations: the state equation (3) and the field equation (4)

$$E^{\mathrm{d}}_{l,p}(\mathbf{r} \in \Gamma) = k^2_{0,p} \int_\Omega \chi_p(\mathbf{r}') E_{l,p}(\mathbf{r}') G_p(\mathbf{r}, \mathbf{r}')\, \mathrm{d}\mathbf{r}', \tag{3}$$

$$E_{l,p}(\mathbf{r} \in \Omega) = E^{\mathrm{inc}}_{l,p}(\mathbf{r}) + k^2_{0,p} \int_\Omega \chi_p(\mathbf{r}') E_{l,p}(\mathbf{r}') G_p(\mathbf{r}, \mathbf{r}')\, \mathrm{d}\mathbf{r}', \tag{4}$$

where G_p denotes the two-dimensional free space Green function, and $\chi_p(\mathbf{r}) = \tilde{\varepsilon}_{r,p}(\mathbf{r}) - 1$, with $\tilde{\varepsilon}_{r,p}(\mathbf{r}) = \varepsilon_{r,p}(\mathbf{r}) - \frac{\mathrm{i}\sigma(\mathbf{r})}{\omega_p \varepsilon_0}$, is the complex permittivity contrast. For the sake of simplicity, equations (3) and (4) are rewritten in more condensed form using symbolic operator notation

$$E^{\mathrm{d}}_{l,p} = \mathbf{K}_p \chi_p E_{l,p}, \tag{5}$$

$$E_{l,p} = E^{\mathrm{inc}}_{l,p} + \mathbf{G}_p \chi_p E_{l,p}. \tag{6}$$

For the inversion, it is assumed that the targets are successively illuminated by $(L \times P)$ excitations, and for each source (l, p), the scattered field $E^{\mathrm{d,mes}}_{l,p}$ is measured on M receivers located on Γ.

3. Inversion schemes

The aim of inverse problems is to determine characteristics of targets present in the investigating domain Ω. It consists in determining the real relative permittivity ε_r and the conductivity σ distributions of the objects such that the measured scattered field $E^{\mathrm{d,mes}}_{l,p}$ on Γ matches the scattered field $E^{\mathrm{d}}_{l,p}$ computed, thanks to the state equation (3) and the field equation (4), with the estimation of ε_r and σ.

In this paper, we propose three different iterative algorithms. They are based on the inversion methods described in [5] and referred to therein as the *modified*^{2}*gradient method* (M^{2}GM), *modified Born method* (MBM), and *modified gradient method* (MGM). In [5], the inversion was carried out for a single frequency. When multiple-frequency data are involved, an efficient strategy for the inversion consists in applying a frequency-hopping approach [1–3], i.e., the initial guess for solving the inverse problem at a high frequency is given by the final result obtained at a lower frequency. This strategy requires at each step the inversion of single-frequency data.

In present paper, we investigate an alternative method to invert multiple-frequency data. We, therefore, extend the inversion schemes in order to process multiple-frequency data. We thus avoid applying the frequency-hopping approach.

3.1. Basic relations

The basic idea underlying the iterative inversion algorithms is to gradually determine the parameters of interest by minimizing at each iteration step a cost functional involving the discrepancy between the measurements, and that would be obtained via a forward model with the estimation of the parameters. In the three inversion schemes (MGM, MBM and M^{2}GM), the expansion coefficients for field and parameters are determined simultaneously. In addition, the parameters (permittivity as well as conductivity) are updated along the standard Polak–Ribière conjugate gradient directions of a cost functional. The difference lies in the choice of the update direction for the field.

3.1.1. Modified gradient method. In MGM three sequences relative to the total field, relative permittivity and conductivity are built up according to the following relations:

$$E_{l,p,n} = E_{l,p,n-1} + \alpha_{l,p,n;v} v_{l,p,n}, \tag{7}$$

$$\xi_n = \xi_{n-1} + \beta_{n;\xi} d_{n;\xi}, \tag{8}$$

$$\eta_n = \eta_{n-1} + \beta_{n;\eta} d_{n;\eta}, \tag{9}$$

where ξ and η are frequency-independent real-valued functions and defined as $\chi_p = \xi^2 - \frac{i\eta^2}{\omega_p \varepsilon_0}$. Note that, with this definition of the contrast χ_p, a positivity constraint on the conductivity ($\sigma = \eta^2$) and on the electrical susceptibility (ξ^2, with $\varepsilon_r = 1 + \xi^2$) is inherently imposed. $v_{l,p,n}$, $d_{n;\xi}$ and $d_{n;\eta}$ are update directions which will be given precisely later in the paper. $\alpha_{l,p,n;v} \in \mathbb{C}$ and $\beta_{n;\xi}, \beta_{n;\eta} \in \mathbb{R}$ are scalars coefficients determined at each iteration such that they minimize the normalized cost functional $\mathcal{F}$ given by

$$\mathcal{F}_n(E_{l,p,n}; \xi_n; \eta_n) = W_\Omega \cdot \sum_{p=1}^{P} \sum_{l=1}^{L} \left\| h^{(1)}_{l,p,n} \right\|^2_\Omega + W_\Gamma \cdot \sum_{p=1}^{P} \sum_{l=1}^{L} \left\| h^{(2)}_{l,p,n} \right\|^2_\Gamma, \tag{10}$$

where the normalizing coefficients are defined as

$$W_\Omega = \frac{1}{\sum_{p=1}^{P} \sum_{l=1}^{L} \left\| E^{\text{inc}}_{l,p} \right\|^2_\Omega}, \qquad W_\Gamma = \frac{1}{\sum_{p=1}^{P} \sum_{l=1}^{L} \left\| E^{\text{d,mes}}_{l,p} \right\|^2_\Gamma}. \tag{11}$$

Subscripts Ω and Γ included in the norm $\|\cdot\|$ and later in the inner product $\langle \cdot, \cdot \rangle$ indicate the domain of integration. The two functions $h^{(1)}_{l,p,n}$ and $h^{(2)}_{l,p,n}$ are the residual errors computed from the field and the state equations, respectively. They are given by

$$h^{(1)}_{l,p,n} = E^{\text{inc}}_{l,p,n} - E_{l,p,n} + \mathbf{G}_p \chi_{p,n} E_{l,p,n}, \tag{12}$$

$$h^{(2)}_{l,p,n} = E^{\text{d,mes}}_{l,p} - \mathbf{K}_p \chi_{p,n} E_{l,p,n}. \tag{13}$$

Substituting, in the cost functional defined in equation (10), the expressions of the field and the parameters, defined in equations (7), (8) and (9), leads to a polynomial expansion of the cost function $\mathcal{F}_n$ with $(L \times P)$ complex variables $\alpha_{l,p,n;v}$ and two real variables $\beta_{n;\xi}, \beta_{n;\eta}$. The minimization of this cost function is accomplished using the standard Polak–Ribière conjugate gradient procedure [6].

As update directions for the parameters $d_{n;\xi}$ and $d_{n;\eta}$, the authors take the standard Polak–Ribière conjugate gradient directions. These read

$$d_{n;\xi} = g_{n;\xi} + \gamma_{n;\xi} d_{n-1;\xi} \qquad \text{with} \qquad \gamma_{n;\xi} = \frac{\langle g_{n;\xi}, g_{n;\xi} - g_{n-1;\xi} \rangle_\Omega}{\|g_{n-1;\xi}\|^2_\Omega}, \tag{14}$$

$$d_{n;\eta} = g_{n;\eta} + \gamma_{n;\eta} d_{n-1;\eta} \qquad \text{with} \qquad \gamma_{n;\eta} = \frac{\langle g_{n;\eta}, g_{n;\eta} - g_{n-1;\eta} \rangle_\Omega}{\|g_{n-1;\eta}\|^2_\Omega}, \tag{15}$$

where $g_{n;\xi}$ and $g_{n;\eta}$ are the gradient of the functional $\mathcal{F}$ with respect to ξ and η assuming that the field does not change.

$$g_{n;\xi} = 2\xi_{n-1} \,\text{Re}\left(W_\Omega \sum_{p=1}^{P} \sum_{l=1}^{L} E^*_{l,p,n-1} \mathbf{G}^\dagger_p h^{(1)}_{l,p,n-1} + W_\Gamma \sum_{p=1}^{P} \sum_{l=1}^{L} E^*_{l,p,n-1} \mathbf{K}^\dagger_p h^{(2)}_{l,p,n-1} \right), \tag{16}$$

$$\begin{aligned} g_{n;\eta} = -2\eta_{n-1} \,\text{Im}\Bigg(& W_\Omega \sum_{p=1}^{P} \frac{1}{\omega_p \varepsilon_0} \sum_{l=1}^{L} E^*_{l,p,n-1} \mathbf{G}^\dagger_p h^{(1)}_{l,p,n-1} \\ & + W_\Gamma \sum_{p=1}^{P} \frac{1}{\omega_p \varepsilon_0} \sum_{l=1}^{L} E^*_{l,p,n-1} \mathbf{K}^\dagger_p h^{(2)}_{l,p,n-1} \Bigg), \end{aligned} \tag{17}$$

where $*$ denotes the complex conjugate and $\mathbf{G}^\dagger_p$ and $\mathbf{K}^\dagger_p$ are the adjoint operators of $\mathbf{G}_p$ and $\mathbf{K}_p$, respectively.

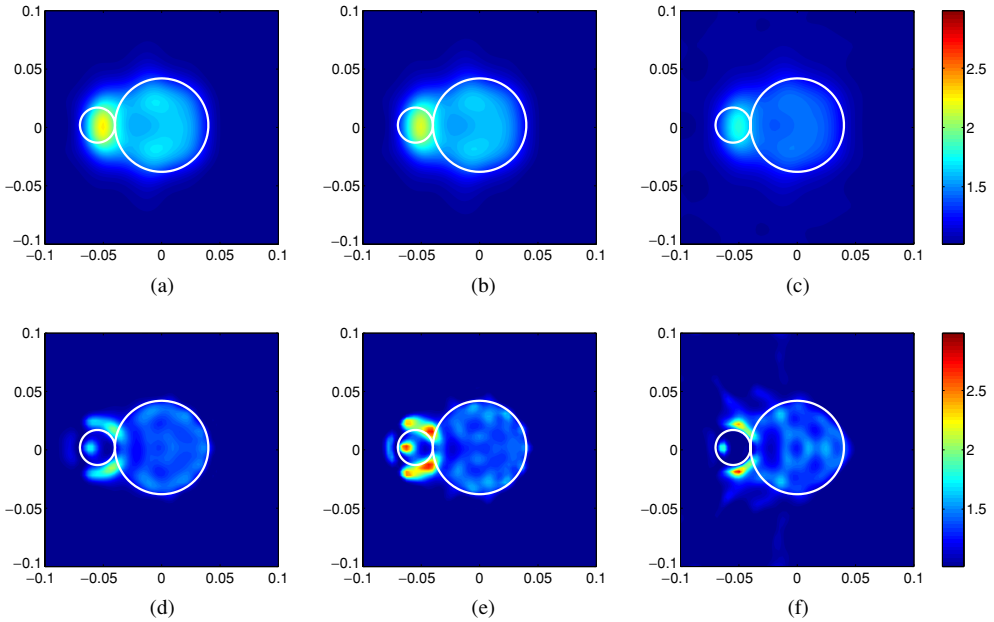

Figure 2. Reconstructed permittivity profile of the two dielectric cylinders 'FoamDielExt; one outside the other. The inversion is carried out with the minimization of the cost function $\mathcal{F}$. (a), (d) M^2GM; (b), (e) MGM; (c), (f) MBM. The first row corresponds to the frequency band 2–5 GHz, while the second row corresponds to 2–8 GHz.

The update direction $v_{l,p,n}$ for the total field is similar to those chosen for ξ_n and η_n.

$$v_{l,p,n} = g_{l,p,n;E} + \gamma_{l,p,n;E} v_{l,p,n-1}$$

with

$$\gamma_{l,p,n;E} = \frac{\langle g_{l,p,n;E},\, g_{l,p,n;E} - g_{l,p,n-1;E}\rangle_\Omega}{\|g_{l,p,n-1;E}\|_\Omega^2}. \tag{18}$$

In this relation, $g_{l,p,n;E}$ corresponds to the gradient of the functional $\mathcal{F}_n$ with respect to $E_{l,p,n}$ assuming that the contrast in Ω does not change.

$$g_{l,p,n;E} = W_\Omega\left(\chi^*_{p,n-1}\mathbf{G}_p^\dagger h^{(1)}_{l,p,n-1} - h^{(1)}_{l,p,n-1}\right) - W_\Gamma \chi^*_{p,n-1}\mathbf{K}_p^\dagger h^{(2)}_{l,p,n-1}. \tag{19}$$

3.1.2. Modified Born method. In this method, the same recursive relations (8) and (9) associated with the contrast permittivity are used. The changes lie in the update direction for the field.

$$E_{l,p,n} = E_{l,p,n-1} + \alpha_{l,p,n;w} w_{l,p,n}, \tag{20}$$

where the field update direction $w_{l,p,n}$ is of the form

$$w_{l,p,n} = \tilde{E}_{l,p,n-1} - E_{l,p,n-1}. \tag{21}$$

$\tilde{E}_{l,p,n}$ corresponds to the field solution of equation (6) with the contrast $\chi_{p,n-1}$. It is computed iteratively using the CGFFT (conjugate gradient fast Fourier transform) method into which an extrapolation procedure (marching on in frequency) is plugged generating an initial guess to accelerate the convergence of the iterative process. Details of this fast forward solver are given in [7].

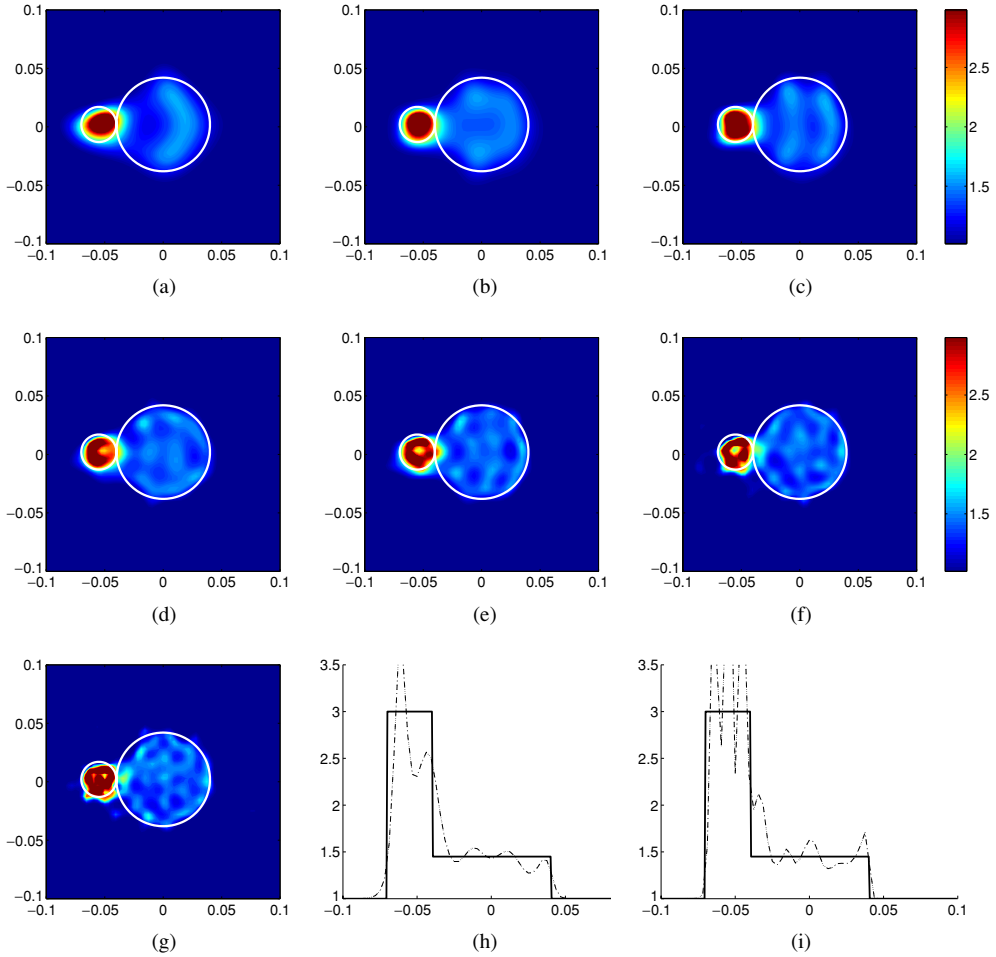

Figure 3. Reconstructed permittivity profile of the two dielectric cylinders 'FoamDielExt'. The inversion is obtained using the frequency-hopping approach with M^{2}GM. (a) $f = 2$ GHz; (b) $f = 3$ GHz; (c) $f = 4$ GHz; (d) $f = 5$ GHz; (e) $f = 6$ GHz; (f) $f = 7$ GHz; (g) $f = 8$ GHz. (h) Comparison, along the line $y = 0$, between the reconstructed profile at $f = 5$ GHz (- - - -) and the actual one (——). (i) Same as in (h) but for $f = 8$ GHz.

The cost function $\mathcal{F}_n$ is as for MGM a polynomial of $(L \times P)$ complex variables and two reals. The minimization of this cost function remains unchanged.

3.1.3. Modified modified gradient method. This last method is a 'hybridization' of the two aforementioned ones. The recursive relation associated with the total field in Ω is now a combination of (7) and (20).

$$E_{l,p,n} = E_{l,p,n-1} + \alpha_{l,p,n;v} v_{l,p,n} + \alpha_{l,p,n;w} w_{l,p,n}, \tag{22}$$

where $v_{l,p,n}$ is the same as in (18) while $w_{l,p,n}$ is the same as (21). Complex coefficients $\alpha_{l,p,n;v}$ and $\alpha_{l,p,n;w}$ are obtained by minimizing the polynomial cost function $\mathcal{F}_n$ with $2 \times (L \times P)$ complex variables and still two reals.

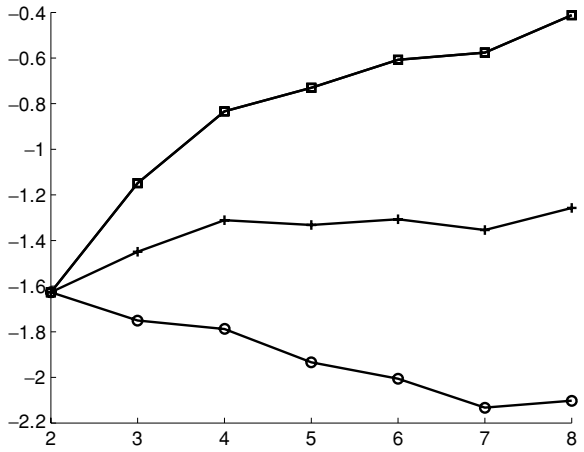

Figure 4. Evolution of $u(p)$, $u(p)/p$ and $u(p)/p^2$ (log-scale representation) versus the frequency in GHz. (□) $u(p)$; (+) $u(p)/p$ and (○) $u(p)/p^2$.

3.1.4. Initial guess. Due to the positivity constraint, the initial guess ($\xi_0 = 0$; $\eta_0 = 0$) must be rejected since the gradients vanish. Thus, we need another initial guess. This can be provided by the back-propagation method [8–10]. As an initial guess for the field, the authors take the field solution of equation (4) with the permittivity contrast derived by the back-propagation method.

4. Numerical experiments

Results of the reconstruction of two-dimensional inhomogeneous objects from experimental data are reported in the present section. As mentioned above, we restrict ourselves to the case of TM-polarized fields. All the data were provided courtesy of Institut Fresnel (Marseille, France). The parameters of the experimental set-up needed for inversion as well as the database are described in [11]. To sum up briefly, the multiple-frequency data correspond to $L = 8$ or 18 (depending on the target under test) different source positions evenly distributed along a circle with radius 1.67 m. The $M = 241$ receivers were also evenly distributed along the same circle as for the sources, with, however, an exclusion area of 120° angular sector. This exclusion area is inherent to the mechanical encumbrance of the experimental set-up. The number of frequencies may vary from one set to another. For the inversion, we used in all cases two subsets with a fixed frequency step $\Delta f = 1$ GHz: a narrow frequency band 2–5 GHz (with $P = 4$) and a wider one 2–8 GHz (with $P = 7$). The incident field used in the inversion (TM-polarized field generated by a line source) was calibrated for each frequency from the measured incident field when the receiver and the transmitter face each other. All the initial guesses are obtained as specified in section (3.1.4), except when the frequency-hopping approach is applied. All the reported final results correspond to the 50th iteration. This stopping criterion was motivated firstly by our wish to compare the different methods at the same stage and secondly by the need to carry out enough iterations to obtain significant results. Furthermore, we did not note any marked changes in the results when continuing iterating. The test domain Ω used in the reconstruction was in all cases a large square box of size 20×20 cm^2 centred at the origin and discretized for numerical purposes into 64×64 square cells.

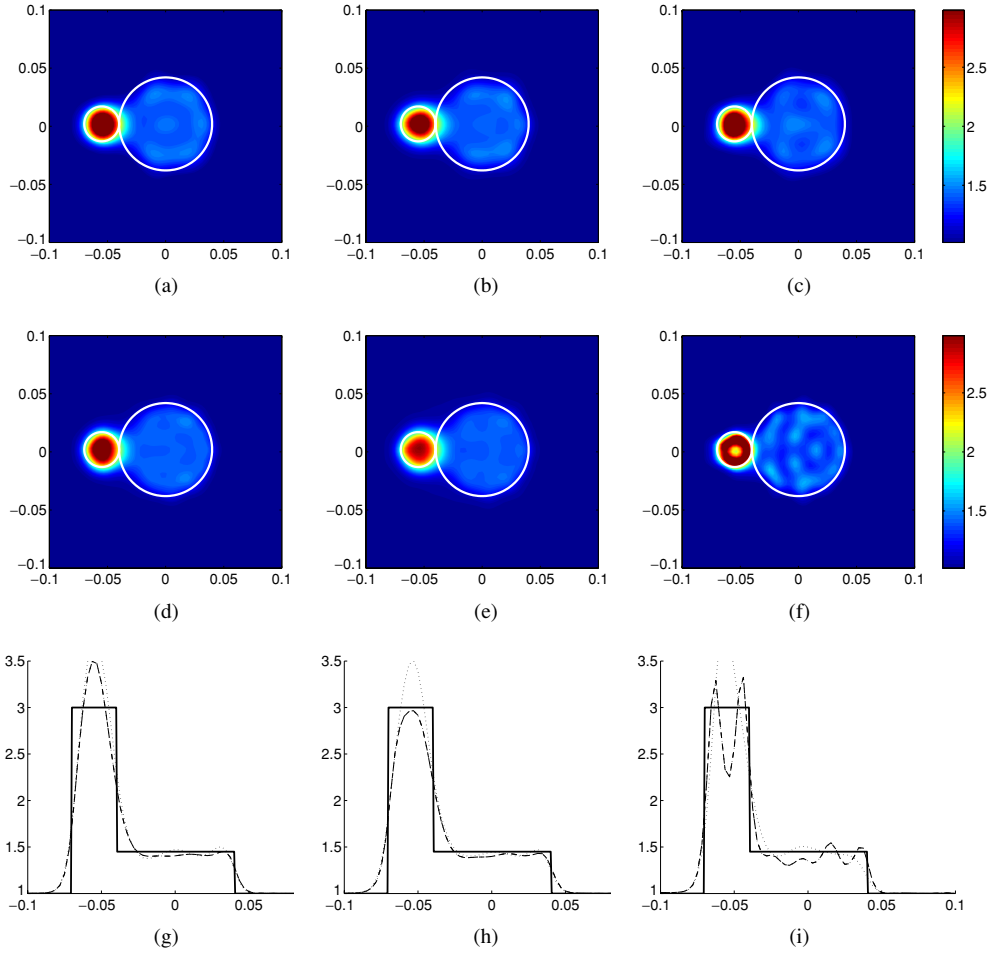

Figure 5. Reconstructed permittivity profile of the two dielectric cylinders 'FoamDielExt'; one outside the other. The inversion is carried out with the minimization of the cost function $\mathcal{F}_{(1/p^2)}$. (a), (d) M^{2}GM; (b), (e) MGM; (c), (f) MBM. The first row corresponds to the frequency band 2–5 GHz, while the second row corresponds to 2–8 GHz. The third row presents a comparison between the reconstructed profile and the actual one along the line $y = 0$: (——) actual profile, (· · · · · ·) 2–5 GHz and (- - - -) 2–8 GHz.

To avoid specifying in the text the geometry and the permittivity of the targets under test, their boundary is plotted in the figures (white circles), as well as a cut of the map of permittivity.

4.1. Inversion strategy: multiple-frequency, frequency-hopping approach

In this section, we present several strategies to invert multiple-frequency data. These strategies have been applied to all the targets of the database. Due to the large number of results, their comparison is restricted to one set only, keeping in mind that the same conclusions hold also for the other sets. The target under test, referred in the database to as FoamDielExt, is composed of two dielectric circular cylinders, one outside the other. For this target $L = 8$ and only the reconstructed permittivity is represented. In figure 2 are reported results of the reconstruction using M^{2}GM, MGM and MBM when all the multiple-frequency data are processed at the

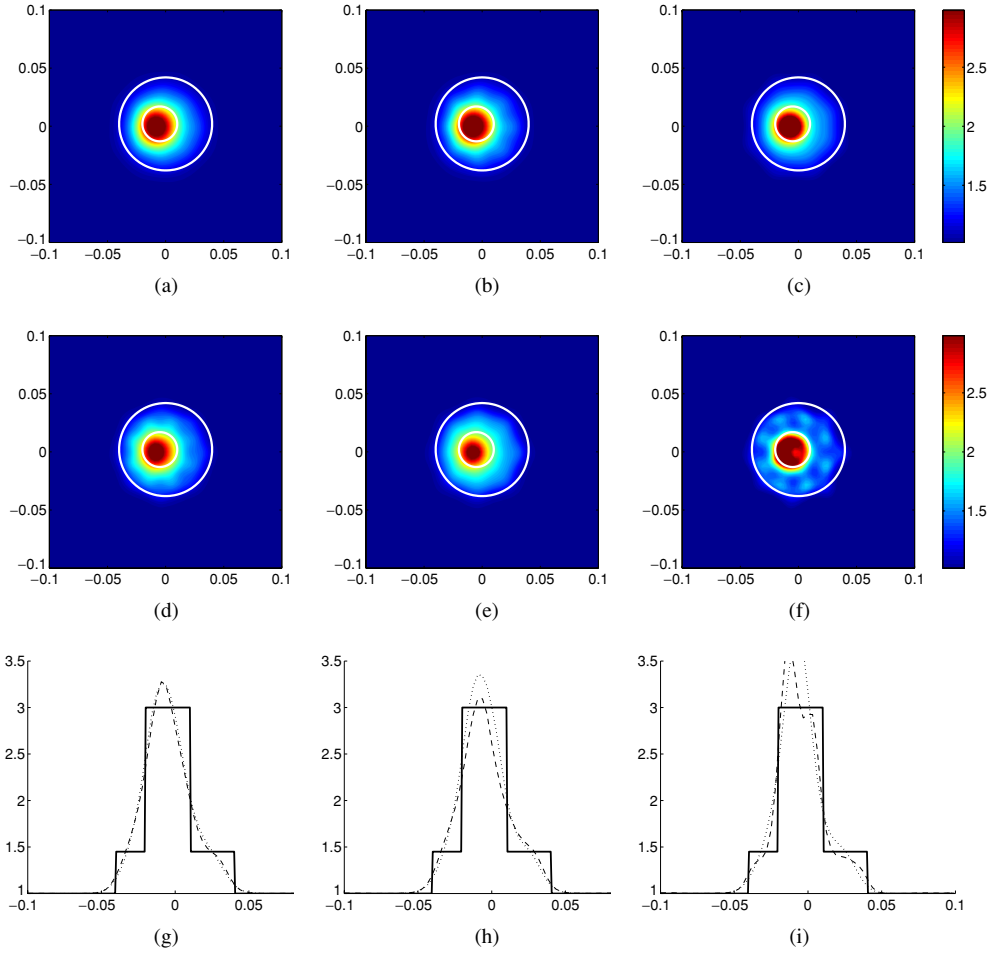

Figure 6. Reconstructed permittivity profile of the two dielectric cylinders 'FoamDielInt'. The inversion is carried out with the minimization of the cost function $\mathcal{F}_{(1/P^2)}$. (a), (d) and (g) M^{2}GM; (b), (e) and (h) MGM; (c), (f) and (i) MBM. The first row corresponds to the frequency band 2–5 GHz, while the second row corresponds to 2–8 GHz. The third row presents a comparison between the reconstructed profile and the actual one along the line $y = 0$: (——) actual profile, (· · · · · ·) 2–5 GHz and (- - - -) 2–8 GHz.

same time. The results are disappointing with both frequency bands 2–5 GHz and 2–8 GHz. The schemes did not even succeed in determining whether the target under test is dielectric or metallic since the maximum value of the reconstructed conductivity is as high as $\sigma^{\max} = 4.2$, 2.2 and 1.5 S m^{-1} for M^{2}GM, MGM and MBM, respectively—the corresponding reconstructed permittivity is plotted in figures 2(d)–(f), respectively. For such a value of the conductivity, one may deduce that the target under test is partly made of metal.

Several reasons may explain why the inversion algorithm fails at providing satisfactory results.

- The signal-to-noise ratio is so small that the information related to the parameters is just not accessible.

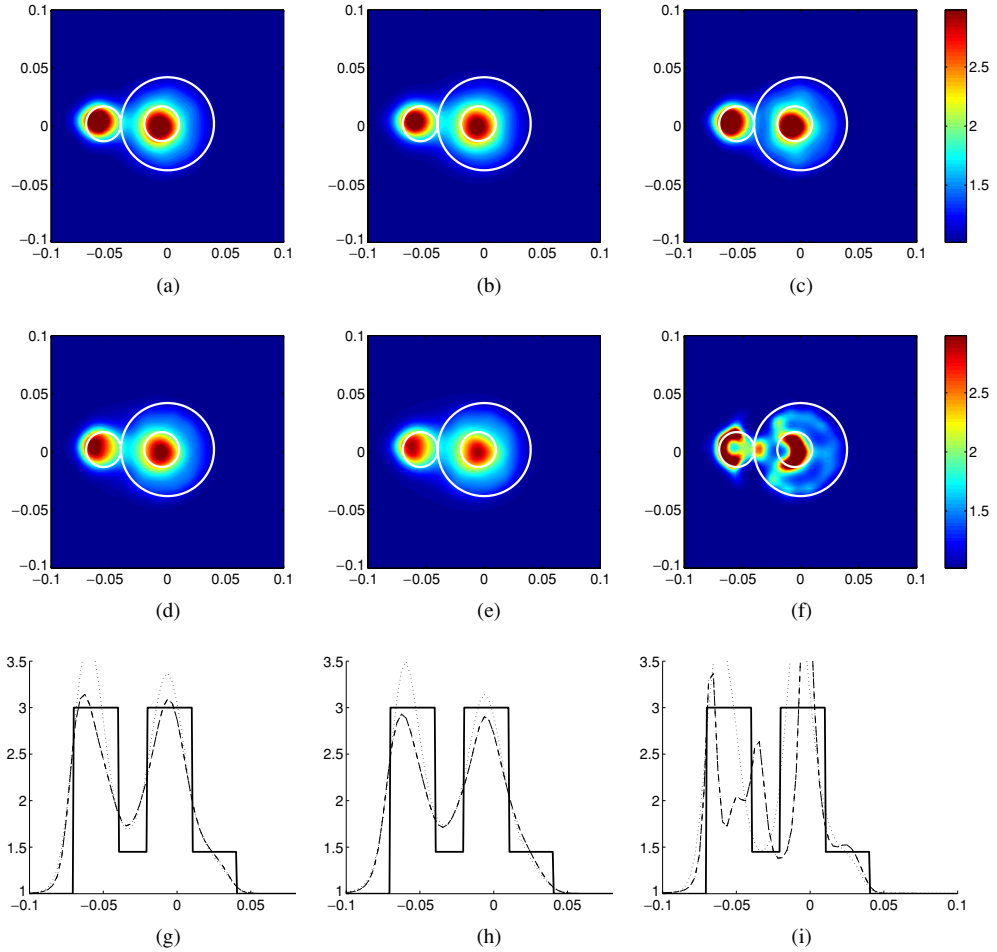

Figure 7. Reconstructed permittivity profile of the three dielectric cylinders 'FoamTwinDiel'. Two of them are identical; one inside and the other outside the foam cylinder. The inversion is carried out with the minimization of the cost function $\mathcal{F}_{(1/P^2)}$. (a), (d) and (g) M^{2}GM; (b), (e) and (h) MGM; (c), (f) and (i) MBM. The first row corresponds to the frequency band 2–5 GHz, while the second row corresponds to 2–8 GHz. The third row presents a comparison between the reconstructed profile and the actual one along the line $y = 0$: (——) actual profile, (· · · · · ·) 2–5 GHz and (- - - -) 2–8 GHz.

- The contribution from high frequencies in the minimized cost function strongly dominates, thus leading us to invert only the high-frequency data, for which it is well known that the iterative algorithms badly support the convergence [1].

Let us examine the frequency-hopping approach. The results of the reconstruction using M^{2}GM are plotted in figure 3. Satisfactory reconstructions are obtained, with improved resolution when increasing the frequency in the 2–5 GHz frequency range considered in figure 2. These results clearly contradict the hypothesis related to the signal-to-noise ratio.

Higher frequencies do not bring any improvement. This may be due to the fact that the frequency step, $\Delta f = 1$ GHz, is too large to make the iterative scheme converge at high frequencies. To circumvent this, one may reduce the frequency step or include a regularization

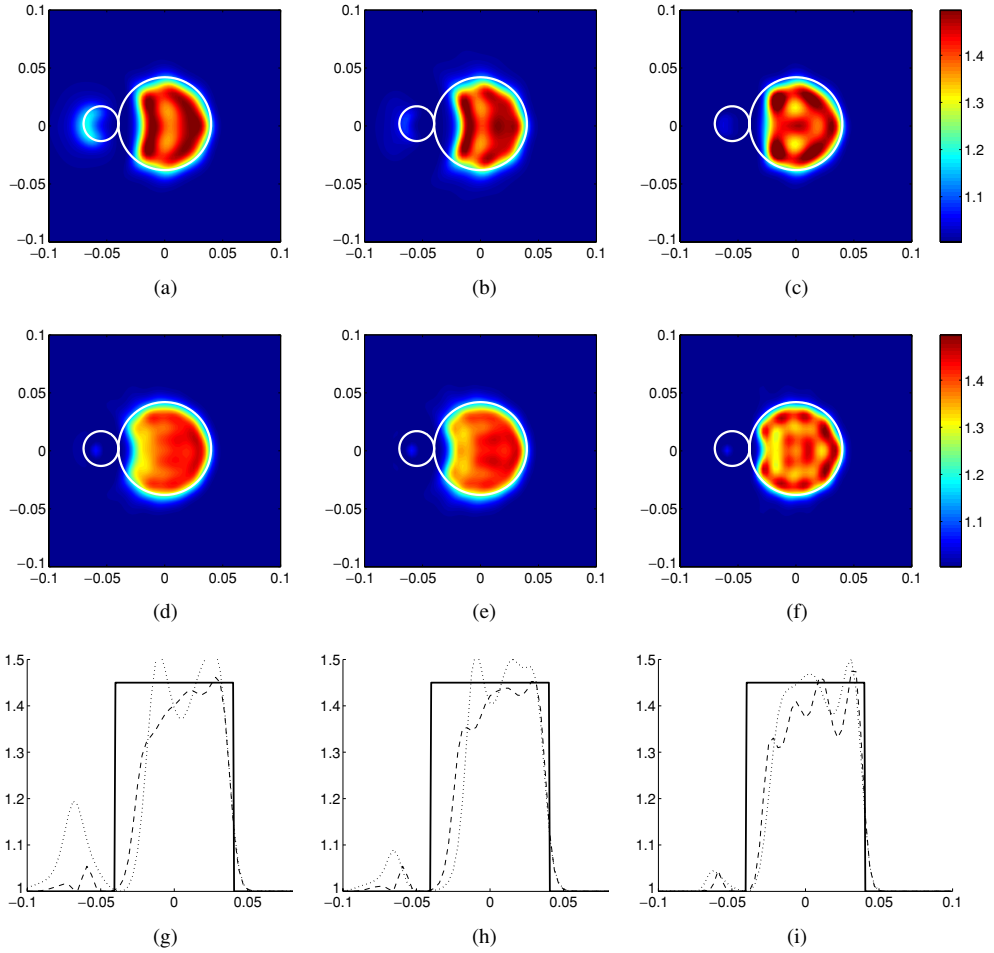

Figure 8. Reconstructed permittivity profile of the two cylinders 'FoamMetExt'; one is dielectric while the other is metallic. The inversion is carried out with the minimization of the cost function $\mathcal{F}_{(1/P^2)}$. (a), (d) and (g) M^{2}GM; (b), (e) and (h) MGM; (c), (f) and (i) MBM. The first row corresponds to the frequency band 2–5 GHz, while the second row corresponds to 2–8 GHz. The third row presents comparisons between the reconstructed profile (- - - -) and the actual one (——).

procedure in the inversion scheme. Indeed, it has been shown that including regularization procedures in iterative inverse schemes improves the resolution (see for instance [12], where a total variation (TV) type regularization was applied to the modified gradient method or [13] where an edge-preserving (EP) regularization is applied to the same inverse scheme).

The behaviour at high frequencies deserves some attention. Let us examine the weight of the measurements with respect to frequency, more precisely the evolution of the quantity $u(p)$

$$u(p) = \sum_{l=1}^{L} \left\| E_{l,p}^{\mathrm{d,mes}} \right\|_{\Gamma}^{2}. \tag{23}$$

Figure 4 presents the evolution of $u(p)$, $u(p)/p$ and $u(p)/p^2$ versus frequency. It suggests weighting the minimized cost function (10) by a factor $1/p$, which, according to what is

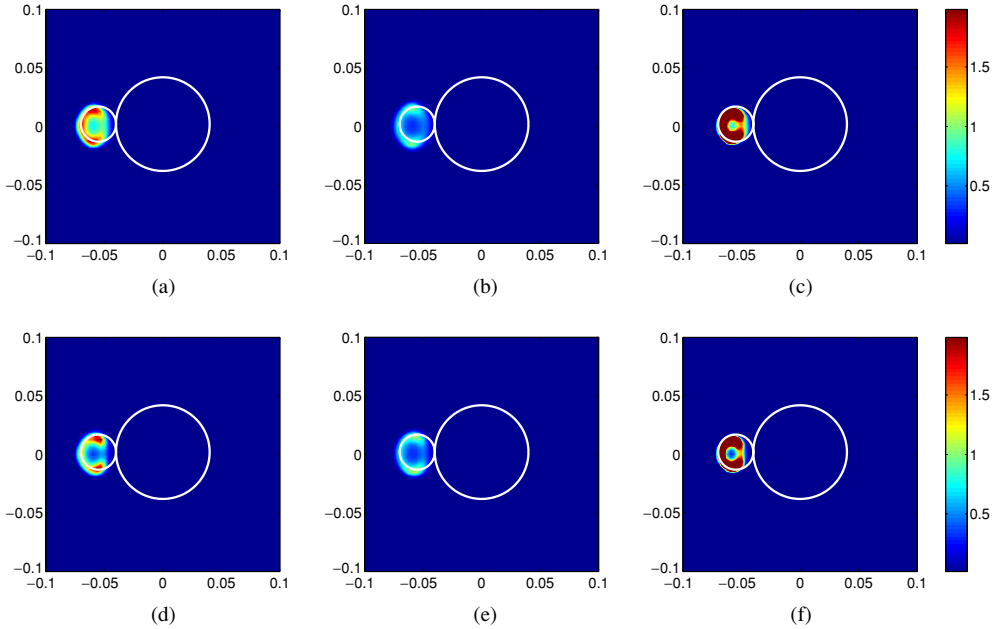

Figure 9. Reconstructed conductivity profile of the two cylinders 'FoamMetExt'; one is metallic and the other is purely dielectric. The inversion is carried out with the minimization of the cost function $\mathcal{F}_{(1/P^2)}$. (a), (d) M^{2}GM; (b), (e) MGM; (c), (f) MBM. The first row corresponds to the frequency band 2–5 GHz, while the second row corresponds to 2–8 GHz.

observed in figure 4, corresponds to somehow treating all frequencies evenly. Our suggestion is to change the minimized cost function into

$$\mathcal{F}_{(1/P)} = \frac{\sum_{p=1}^{P}(1/p)\sum_{l=1}^{L}\left\|h_{l,p}^{(1)}\right\|_{\Omega}^{2}}{\sum_{p=1}^{P}(1/p)\sum_{l=1}^{L}\left\|E_{l,p}^{\mathrm{inc}}\right\|_{\Omega}^{2}} + \frac{\sum_{p=1}^{P}(1/p)\sum_{l=1}^{L}\left\|h_{l,p}^{(2)}\right\|_{\Gamma}^{2}}{\sum_{p=1}^{P}(1/p)\sum_{l=1}^{L}\left\|E_{l,p}^{\mathrm{d,mes}}\right\|_{\Gamma}^{2}}. \tag{24}$$

The results of the reconstruction with the cost function $\mathcal{F}_{(1/P)}$ were satisfactory with the frequency band 2–5 GHz, but disappointing with 2–8 GHz, for which the maximum value of the reconstructed conductivity is smaller than previously, but still high ($\sigma^{\max} = 0.16$, 0.33 and 0.91 S m^{-1} for M^{2}GM, MGM and MBM, respectively). Pursuing this idea, the cost function is weighted with the next integer power of $1/p$, i.e. minimizing $\mathcal{F}_{(1/P^2)}$

$$\mathcal{F}_{(1/P^2)} = \frac{\sum_{p=1}^{P}(1/p^2)\sum_{l=1}^{L}\left\|h_{l,p}^{(1)}\right\|_{\Omega}^{2}}{\sum_{p=1}^{P}(1/p^2)\sum_{l=1}^{L}\left\|E_{l,p}^{\mathrm{inc}}\right\|_{\Omega}^{2}} + \frac{\sum_{p=1}^{P}(1/p^2)\sum_{l=1}^{L}\left\|h_{l,p}^{(2)}\right\|_{\Gamma}^{2}}{\sum_{p=1}^{P}(1/p^2)\sum_{l=1}^{L}\left\|E_{l,p}^{\mathrm{d,mes}}\right\|_{\Gamma}^{2}}, \tag{25}$$

leads to satisfactory results for both frequency bands 2–5 GHz and 2–8 GHz and for all the schemes. These results are plotted in figure 5. In this case, the maximum value of the reconstructed conductivity is now $\sigma^{\max} = 0.07$, 0.08 and 0.09 S m^{-1} for M^{2}GM, MGM and MBM, respectively.

4.2. Reconstruction of purely dielectric targets

In this section are presented results of the reconstruction of two other targets of the database, FoamDielInt and FoamTwinDiel, using the inversion strategy derived in the previous section,

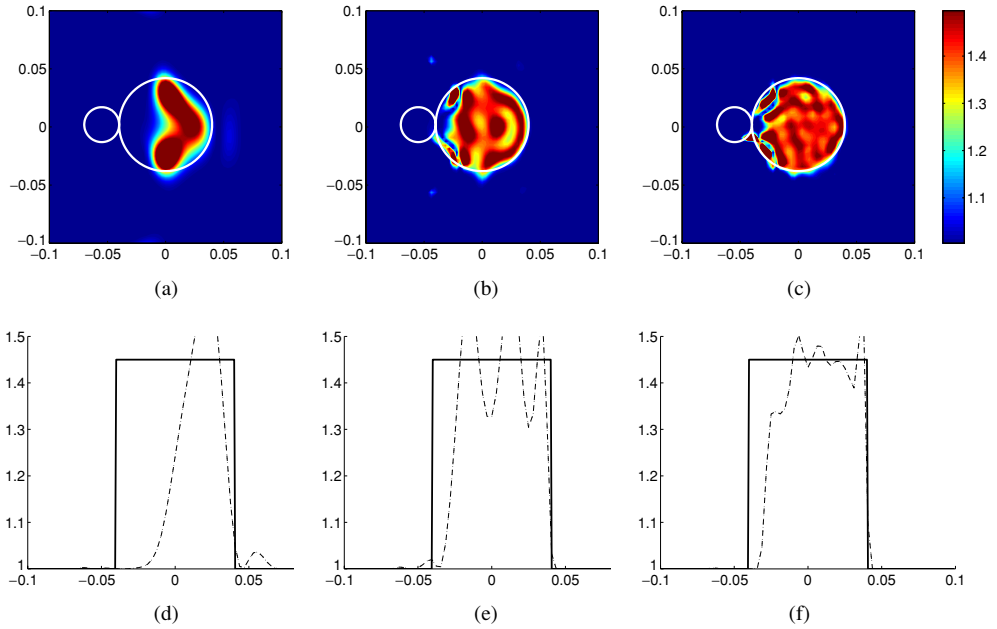

Figure 10. Reconstructed permittivity profile of the two cylinders 'FoamMetExt'; one is metallic and the other is purely dielectric. The inversion is obtained using the frequency-hopping approach with M^{2}GM. (a) $f = 2$ GHz; (b) $f = 5$ GHz; (c) $f = 8$ GHz. (d) Comparison, along the line $y = 0$, between the reconstructed profile at $f = 2$ GHz (- - - -) and the actual one (——); (e) same as in (d) but for $f = 5$ GHz and (f) same as in (d) and (e) but for $f = 8$ GHz.

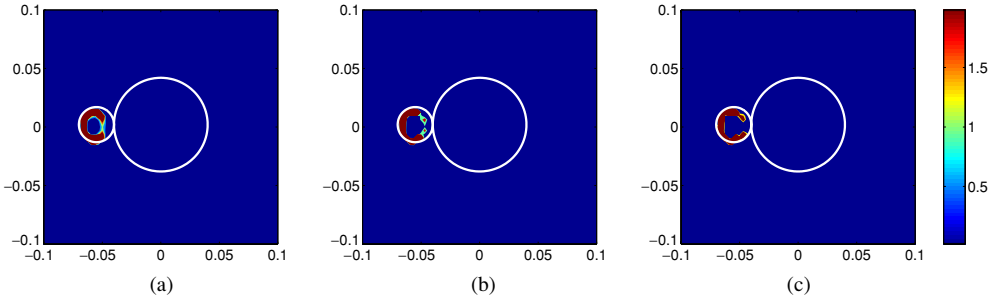

Figure 11. Reconstructed conductivity profile of the two cylinders 'FoamMetExt'; one is metallic and the other is purely dielectric. The inversion is obtained using the frequency-hopping approach with M^{2}GM. (a) $f = 2$ GHz; (b) $f = 5$ GHz and (c) $f = 8$ GHz.

i.e., the inversion of multiple-frequency data with the cost function $\mathcal{F}_{(1/P^2)}$. These results are presented in figures 6 and 7. The target FoamDielInt is constituted of two dielectric cylinders, while FoamTwinDiel is composed of three dielectrics (two of them identical). $L = 8$ and 18 for FoamDielInt and FoamTwinDiel, respectively. For both targets, good results were obtained with all schemes, with, however, a deterioration of the resolution for MBM when switching the frequency band from 2–5 GHz to 2–8 GHz. We should mention that, in the case of target FoamTwinDiel, the reconstruction at $f = 2$ GHz with M^{2}GM allowed us to resolve the two identical cylinders. Note that at this frequency the diameter of the twin cylinders is $\lambda/5$

(λ being the wavelength in vacuum) and that they are separated (distance between the centres) by only $\lambda/3$.

4.3. Reconstruction of metal–dielectric target

In this section are reported results of the reconstruction of an 'exotic' target FoamMetExt that mixes metal and dielectric. Surprisingly, this target was not difficult to reconstruct. Good results were obtained with all schemes without weighting the cost function. However, weighting the cost function improved the results. Figures 8 and 9 present the reconstruction of the permittivity and conductivity profiles with $\mathcal{F}_{(1/P^2)}$. The comparisons between the reconstructed permittivity profiles and the actual one, plotted in figures 8(g)–(i), show that the dielectric constant was correctly retrieved, in particular with M^{2}GM and MGM. The maximum value of the reconstructed conductivity with the frequency band 2–8 GHz, plotted in figure 9, is $\sigma^{\max} = 2.06$, 1.12 and 9.59 S m^{-1} for M^{2}GM, MGM and MBM, respectively. The best result was obtained with MBM. However, such high values of the conductivity lead to a skin depth at $f = 8$ GHz smaller than the mesh size of the solver.

Since the sensitivity to frequency weighting seems much lower with this mixed target, we wondered whether the frequency-hopping approach could be efficient in this case. The corresponding reconstructions are plotted in figures 10 and 11. These figures show the improvement of the resolution for the permittivity profile and almost perfect reconstruction of the boundary of the metallic cylinder even at $f = 2$ GHz. The maximum value of the reconstructed conductivity is much higher than the ones obtained previously ($\sigma^{\max} = 67$, 116 and 163 S m^{-1} at $f = 2, 5$ and 8 GHz, respectively). Amazingly, the strong difference between the scattering strengths of the two neighbouring cylinders does not prevent accurate reconstruction of the low dielectric contrast when multi-frequency data are used.

5. Conclusion

In this paper, three iterative inverse schemes M^{2}GM, MGM and MBM for solving two-dimensional inverse scattering problems have been compared and tested against real multiple-frequency data for several targets, including one mixing metal and dielectric. None of the three presented algorithms uses a regularization procedure. A frequency-weighted cost function was minimized and lead to good results in all cases. Furthermore, the multiple-frequency inversion strategy was compared to the frequency-hopping approach.

References

[1] Tijhuis A G, Belkebir K, Litman A C S and de Hon B P 2001 Theoretical and computational aspects of 2-D inverse profiling *IEEE Trans. Geosci. Remote Sens.* **39** 1316–30

[2] Chew W C and Lin J H 1995 A frequency-hopping approach for microwave imaging of large inhomogeneous bodies *IEEE Microw. Guid. Wave Lett.* **5** 439–41

[3] Tijhuis A G, Belkebir K, Litman A C S and de Hon B P 2001 Multiple-frequency distorted-wave Born approach to 2D inverse profiling *Inverse Problems* **17** 1635–44

[4] Belkebir K and Saillard M 2001 Guest Editors' introduction. Special section: Testing inversion algorithms against experimental data *Inverse Problems* **17** 1565–71

[5] Belkebir K and Tijhuis A G 2001 Modified^2 gradient method and modified Born method for solving a two-dimensional inverse scattering problem *Inverse Problems* **17** 1671–88

[6] Press W H, Flannery B P, Teukolski S A and Vetterling W T 1986 *Numerical Recipes. The Art of Scientific Computing* (Cambridge: Cambridge University Press)

[7] Peng Z Q and Tijhuis A G 1993 Transient scattering by a lossy dielectric cylinder: marching-on-in-frequency approach *J. Electromagn. Waves Appl.* **7** 739–63

[8] Belkebir K, Bonnard S, Pezin F, Sabouroux P and Saillard M 2000 Validation of 2D inverse scattering algorithms from multi-frequency experimental data *J. Electromagn. Waves Appl.* **14** 1637–67

[9] Kleinman R E and van den Berg P M 1994 Two-dimensional location and shape reconstruction *Radio Sci.* **29** 1157–69

[10] Souriau L, Duchêne B, Lesselier D and Kleinman R E 1996 Modified gradient approach to inverse scattering for binary objects in stratified media *Inverse Problems* **12** 463–81

[11] Geffrin J-M, Sabouroux P and Eyraud C 2005 Free space experimental scattering database continuation: experimental set-up and measurement precision *Inverse Problems* **21** S117–30

[12] van den Berg P M and Kleinman R E 1995 A total variation enhanced modified gradient algorithm for profile reconstruction *Inverse Problems* **11** L5–10

[13] Belkebir K, Baussard A and Prémel D 2005 Edge-preserving regularization scheme applied to modified gradient method to reconstruct two-dimensional targets from data laboratory-controlled *Prog. Electromagn. Res.* **54** 1–17